In-plane penetration-depth anisotropy in a *d*-wave model

C. O'Donovan and J. P. Carbotte
Physics and Astronomy Department, McMaster University, Hamilton, Ontario, Canada L8S 4M1
(Received 13 December 1994)

The zero-temperature penetration depth in the CuO_2 plane of $YBa_2Cu_3O_7$ has been found to be very anisotropic. The large measured difference between the *a* and *b* directions is taken as evidence that a significant part of the condensate resides in the chains. We present a simplified model for this anisotropy in which planes (CuO_2) and chains (CuO) are described within a single tight-binding band but with different hopping parameters in the *a* and *b* directions. The pairing is assumed to be due to spin fluctuations in the nearly antiferromagnetic Fermi liquid, but a different mechanism that leads to *d*-wave-type pairing would have similar results.

I. INTRODUCTION

The linear temperature dependence of the low-temperature penetration depth observed[1,2] in high-quality $YBa_2Cu_3O_7$ crystals by microwave techniques[3–5] has been interpreted as evidence for a gap with $d_{x^2-y^2}$ symmetry (in the CuO_2 planes). The observed switchover to a T^2 dependence when Zn impurities[6] are introduced into the CuO_2 planes is understood as due to strong impurity scattering in the unitary limit. Many other experiments have subsequently been interpreted as favoring $d_{x^2-y^2}$ symmetry[7] with nodes and a sign reversal on the diagonal of the two-dimensional (2D) square CuO_2 plane Brillouin zone. In particular, high-resolution (~ 10 meV) angular-resolved photoemission studies (ARPES) in $Bi_2Sr_2CaCu_2O_{8+\delta}$ indicate a zero or near-zero gap on the Fermi surface in the diagonal direction and a maximum in the direction towards the faces[8–11] of the square Brillouin zone. ARPES experiments are not sensitive to the phase of the gap, however, and cannot detect a reversal of sign. Several experiments[12–14] designed specifically to observe this phase have now been reported. One such experiment concludes $d_{x^2-y^2}$ symmetry while another concludes *s* wave. Thus, while the evidence for $d_{x^2-y^2}$ symmetry is certainly strong, this is not a universally held[15–17] view.

Recently, the penetration depth and microwave absorption have been measured separately for the *a* and *b* directions of the CuO_2 plane and found to display a very significant anisotropy.[18,19] For example, the zero-temperature penetration depth in the *a* direction was found to be 1600 Å and in the *b* direction 1030 Å for $YBa_2Cu_3O_{7-\delta}$ (YBCO). This large measured anisotropy has been taken to be the result of the existence of the CuO chains in this material and is taken to be an indication that a considerable amount of the condensate resides on the CuO chains. This is in striking contrast to some suggestions that the chains may be normal.[20–22] A large anisotropy between the *a* and *b* directions has also been observed in the dc resistivity[23–25] and in the thermal conductivity.[26]

Band-structure results based on density-functional theory (DFT) and on the local-density approximation (LDA) for the exchange-correlation energy have revealed[27–29] a complex anisotropic Fermi surface for $YBa_2Cu_3O_{7-\delta}$ with four quasiparticle bands crossing at the Fermi surface. One sheet of the Fermi surface can be identified mainly with the CuO_2 layers, another with the CuO chains, and yet another with a hybridized mixture of chain and plane electrons. Experiments carried out subsequent to the appearance of the band-structure results have largely confirmed the predicted geometry of the Fermi surface for $YBa_2Cu_3O_{7-\delta}$. These include angular correlation of annihilation radiation[30] (ACAR) from positron annihilation studies, angular-resolved photoelectron spectroscopy,[31–33] and even de Haas–Van Alphen (dHvA) experiments.[34]

The dc resistivity anisotropy $\rho_a/\rho_b \sim 2$ for YBCO (Refs. 19, 25) is consistent with the observed anisotropy in the low-frequency limit of the microwave conductivity in the superconducting state,[18,19] with the classical skin-depth effect in the normal state as well as with the normal-state conductivity measurements.[35] Band-structure calculations of the transport properties[36] also indicate a factor of 2 between *a* and *b* directions for the plasma frequency. The inverse of the square of the zero-temperature penetration depth, $[\lambda^2(0)]^{-1}$, is proportional to n/m^* where n is the superfluid fraction and m^* the effective mass. Thus an effective-mass anisotropy of about 2 would also explain the measured anisotropy in λ_a and λ_b.[18,19]

In this paper we present results of calculations of the anisotropic penetration depth in a simplified single-band model which we hope captures some of the essential properties of $YBa_2Cu_3O_{7-\delta}$. To simulate the existence of chains as well as planes we use a tight-binding band but with anisotropic first-nearest-neighbor hopping. This ensures that the *a* and *b* directions are distinct although a single two-dimensional tight-binding copper oxide band is envisaged. For such an anisotropic band structure we write down and solve numerically, by a fast Fourier transform technique, the BCS gap equation with the pairing interaction taken to be due to the exchange of antiferromagnetic spin fluctuations. For the spin susceptibility, which determines the pairing, we employ the simple form

0163-1829/95/52(6)/4568(9)/$06.00

suggested by Millis, Monien, and Pines (MMP).[37–39] This form, which was determined from NMR data, is taken over in our work without modifications and would lead to solutions exhibiting pure $d_{x^2-y^2}$ symmetry[39] for electron energy bands with (K_x,K_y) symmetry (tetragonal). For anisotropic bands, as are envisaged in this work, the numerical solutions are found to contain a mixture of two irreducible representations of the tetragonal point group, namely, $d_{x^2-y^2}$ and $s_{x^2-y^2}$ [containing both isotropic (s_0) and extended s-wave (s_x) components] which, of course, belong to the same irreducible representation of the orthorhombic group. The anisotropy in the band structure and in the resulting gap function leads directly to anisotropy in the penetration depth. It is important to realize that the gap admixture that we use comes out directly from our numerical solutions of the gap equations and is tied to the anisotropy of the assumed band structure. It is not introduced into the theory by any separate group-theoretical considerations. While we have retained in our band structure a single band for simplicity, different effective hopping parameters for a and b directions are meant to simulate the much more complicated multiband nature of YBCO and include in some rough way CuO_2 planes and CuO chains. While the part of the real Fermi surface which originates mainly in the CuO_2 plane is often assumed to have a-b symmetry, the chains definitely do not.

In Sec. II we specify our formalism and present intermediate numerical results for the band structure and for the gap. Section III contains our results for the anisotropic penetration depth. A brief conclusion can be found in Sec. IV.

II. MMP MODEL AND GAP EQUATION

We will assume that the pairing in the copper oxide (CuO_2) plane is due to the exchange of antiferromagnetic spin fluctuations. For the spin susceptibility which describes the coupling between electrons and spin fluctuations, we use the phenomenological model developed by Millis, Monien, and Pines[37] based on consideration of NMR measurements. The static part, which is all that is required in the simplest BCS approach, takes the form

$$\chi(\mathbf{q})=\frac{\chi_0(\mathbf{Q})}{[1+\xi^2(\mathbf{q}-\mathbf{Q})^2]},\quad q_x>0,\quad q_y>0 \tag{1}$$

and is repeated throughout the entire Brillouin zone through symmetry considerations. In Eq. (1) $\mathbf{Q}$ is the commensurate antiferromagnetic wave vector equal to $(\pi/a,\pi/a)$ in the two-dimensional Brillouin zone of the CuO_2 plane with a the lattice parameter. The quantity $\chi_0(\mathbf{Q})$ is a constant which can be absorbed into the arbitrary electron-spin susceptibility coupling g which we will fit to get a value of T_c set around 100 K. This value is representative of the oxides. Finally, ξ is the magnetic coherence length given by Millis, Monien, and Pines and is here left unmodified. The BCS equation based on $\chi(\mathbf{q})$ takes the form

$$\Delta(\mathbf{K})=\frac{1}{\Omega}\sum_{\mathbf{K}'}-g^2\chi(\mathbf{K}-\mathbf{K}')\frac{\tanh[\frac{1}{2}E(\mathbf{K}')/k_BT]}{2E(\mathbf{K}')}\Delta(\mathbf{K}'), \tag{2}$$

where Ω is the volume, k_B Boltzmann's constant, and T the temperature. The quasiparticle energy $E(\mathbf{K})$ in the superconducting state has the form

$$E(\mathbf{K})=\sqrt{\epsilon_{\mathbf{K}}^2+\Delta(\mathbf{K})^2} \tag{3}$$

with $\epsilon_{\mathbf{K}}$ is the dispersion relation for the electrons in a tight-binding band. We write it as

$$\epsilon_{\mathbf{K}}=\bar{t}\{-2[\cos(K_xa)+(1+\delta)\cos(K_yb)] +4B\cos(K_xa)\cos(K_yb)+2(2-2B-\bar{\mu})\}. \tag{4}$$

In Eq. (4) $\bar{t}$ is the in-plane nearest-neighbor hopping matrix element, $\bar{t}B$ is the second-nearest-neighbor hopping, and $\bar{\mu}$ is the chemical potential. It is to be determined from the filling factor $\langle n\rangle$ given by the equation

$$\langle n\rangle=\frac{1}{\Omega}\sum_{\mathbf{K}}\left[1-\frac{\epsilon_{\mathbf{K}}}{E_{\mathbf{K}}}\tanh\left[\frac{E_{\mathbf{K}}}{2k_BT}\right]\right]. \tag{5}$$

The parameter δ in equation (4), which is critical to our work, plays the role of an effective-mass anisotropy parameter and gives a different nearest-neighbor hopping in the a and b directions. As discussed in the Introduction, the real Fermi surface of $YBa_2Cu_3O_{7-\delta}$ has four overlapping bands. While the part coming from the CuO_2 planes has approximate tetragonal symmetry, the part associated mainly with the chains of the CuO plane does not. Rather than introducing several bands into the calculations we retain a single band but put in a-b asymmetry through the parameter δ. While this procedure is certainly not exact, it is the simplest way to introduce the anisotropy into the band structure with a single parameter while, at the same time, preserving much of the simplicity of the previous much based models ($\delta=0$) having tetragonal symmetry.

Lenck and Carbotte[39] have already solved numerically, using a fast Fourier transform technique, the BCS gap equation (1) for a model dispersion (4) with tetragonal symmetry ($\delta=0$) and find that the numerical solution for the gap contains the single irreducible representation of the crystal lattice group with $d_{x^2-y^2}$ symmetry. Of course, the numerical solutions involve many higher harmonics within this representation but much of the physics can be understood using the simple function

$$\Delta(\mathbf{K})\cong\Delta_0(T)[\cos(K_xa)-\cos(K_ya)].$$

When anisotropy is included through δ the solutions for the gap $\Delta(\mathbf{K})$ become more complicated as we will now describe. In Fig. 1 we show the energy surface for $\epsilon_{\mathbf{K}}$ against $\mathbf{K}$ in the $2D$ Brillouin zone of the CuO_2 plane. In this figure $B=0.45$, $\bar{t}=100$ meV, $\delta=0.25$, and the filling is $\langle n\rangle=0.86$ which corresponds to a chemical potential at zero temperature of $\bar{\mu}=0.51$. The Fermi line is shown in the projection plane below the energy surface. Note that we have assembled the Fermi contour around the

corner of the Brillouin zone at $(\pi/a,\pi/a)$ which falls at the center of Fig. 1. The Fermi contour clearly comes closer to the Brillouin zone boundary in the K_x direction than it does in the K_y direction and the K_x and K_y directions are not equivalent. The figure does not have tetragonal symmetry.

While the anisotropy that is clearly seen to exist between the a and b axes in Fig. 1 is not large, it is sufficient to give a gap which does not possess pure $d_{x^2-y^2}$ symmetry as shown in Fig. 2. What is shown in this figure is the gap $\Delta(\mathbf{K})$ as a function of momentum $\mathbf{K}$ in the first Brillouin zone which we obtained from a fast Fourier transform numerical solution of Eq. (1) with no restriction imposed on the gap symmetry. In the projection plane below the gap surface we show the contours of zero gap and see that they are quite different from the case with full tetragonal symmetry (i.e., a pure d-wave gap). For tetragonal symmetry the zeros would fall on the two main diagonals. When we projected our solution onto the various irreducible representations of the tetragonal group we found that it contained a mixture of $d_{x^2-y^2}$, isotropic (s_0), and extended s-wave (s_x) representation. From now on, we will refer to the s-wave part as the sum of constant (s_0) and extended s (denoted by s_x), so $s \equiv s_0 + s_x$. In our numerical solutions, the d-wave part contains many higher harmonics besides the usual $[\cos(K_x a)-\cos(K_y a)]$ part and so does the extended s_x-wave part. It consists of a $[\cos(K_x a)+\cos(K_y a)]$ part plus many higher harmonics. In Fig. 3, we show the projected s-wave part which, we repeat, contains a small constant part and many extended $s\,(s_x)$ higher harmonics. In Fig. 4, the d-wave part is projected out for the convenience of the reader. It is not a simple $[\cos(K_x a)-\cos(K_y a)]$ function. Nevertheless, a reasonable, although certainly not exact, fit to the solution of Fig. 2 can be written as

$$\Delta(\mathbf{K})=\Delta_0(T)\{\eta_d+0.25\eta_{S_x}+\text{small constant part}\} \quad (6)$$

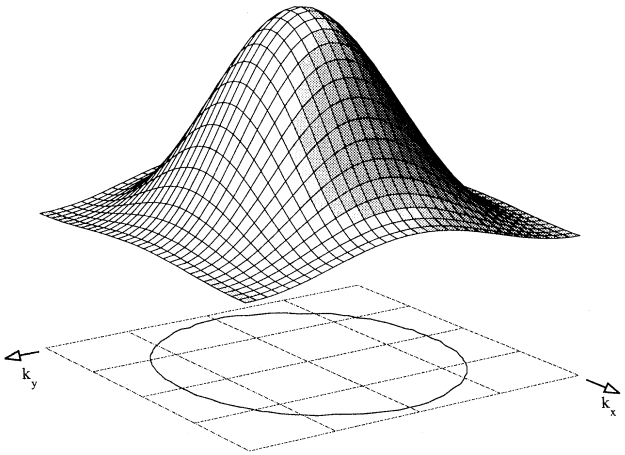

FIG. 1. Electron energy surface $\epsilon(\mathbf{K})$ as a function of momentum (K_x,K_y) in the first Brillouin zone of the copper oxide plane. We have used Eq. (4) with $B=0.45$, $\delta=0.25$, and $\langle n\rangle=0.86$. Also shown in the projection plane is the Fermi contour. The point $(\pi/a,\pi/a)$ is at the center of the figure.

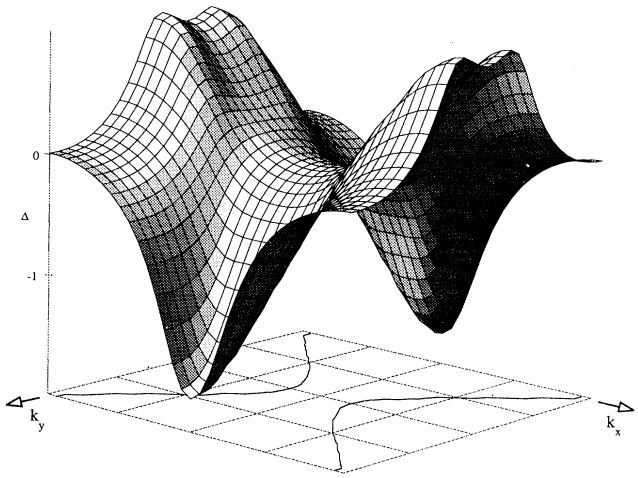

FIG. 2. Gap surface $\Delta(\mathbf{K})$ as a function of momentum (K_x,K_y) in the first Brillouin zone of the copper oxide plane obtained from a numerical solution of the BCS gap equation (2) with $g^2\chi_0$ adjusted to get $T_c=94$ K. The spin susceptibility is fixed to its value given by MMP.[37] The electron dispersion is given by (4) with $B=0.45$, $\delta=0.25$, and $\langle n\rangle=0.86$. Shown in the projection plane are the contours of zero gap. Note how different this is from the case with $\delta=0$, the tetragonal symmetry, in which instance the zeros would be on the diagonals of the Brillouin zone. In our case with $\delta\neq 0$, the gap $\Delta(\mathbf{K})$ is a mixture of a main $d_{x^2-y^2}$ component and a weaker constant (s_0) plus extended s-wave (s_x) component.

where

$$\eta_d=[\cos(K_x a)-\cos(K_y a)]$$

and

$$\eta_{s_x}=[\cos(K_x a)+\cos(K_y a)]\ ,$$

and could be used as a simplified model for our numerical

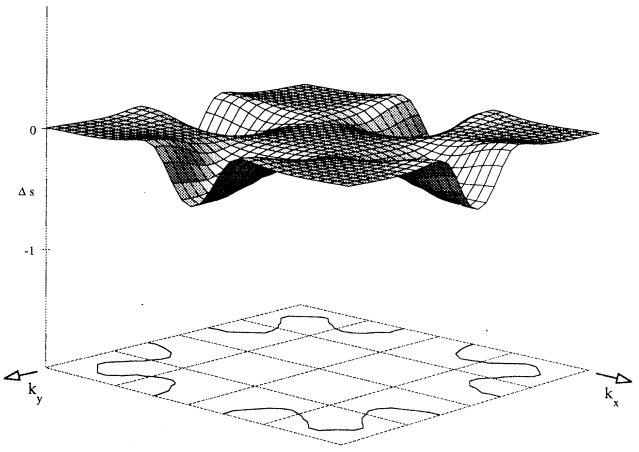

FIG. 3. The projected S part of the complete numerical solution $\Delta(\mathbf{K})$ shown in Fig. 2 given as a function of momentum (K_x,K_y) of the first Brillouin zone of the CuO_2 plane. The projection plane shows the zero contours for this projection, which contains a constant part (s_0) plus an extended s-wave (s_x) piece. The extended s_x piece contains many higher harmonics of this irreducible representation.

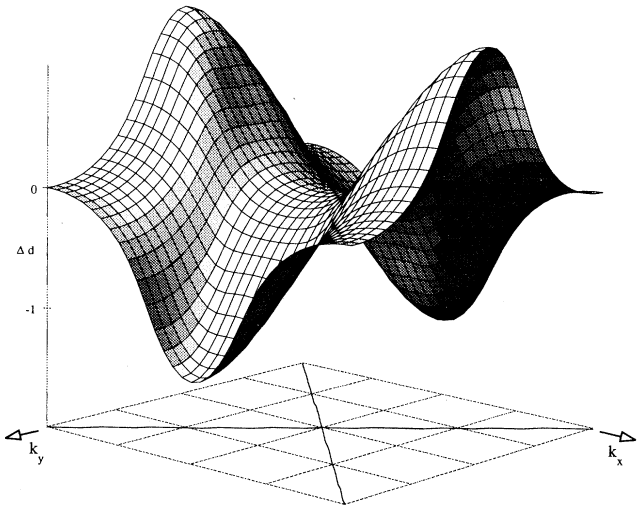

FIG. 4. The projected d part of the complete numerical solution $\Delta(\mathbf{K})$ shown in Fig. 2 given as a function of momentum (K_x,K_y) of the first Brillouin zone of the CuO_2 plane. The projection plane shows the zero contours for this projection which are on the main diagonals of the first Brillouin zone. The d-wave part with $d_{x^2-y^2}$ symmetry contains many higher harmonics of this irreducible representation.

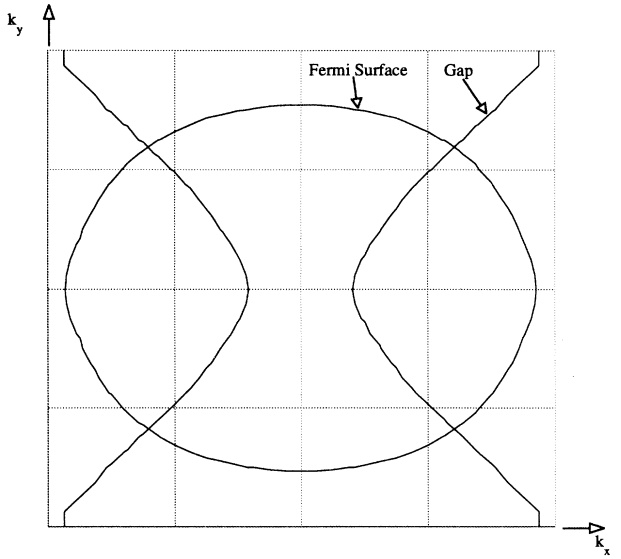

FIG. 5. The contours of zero gap superimposed on the Fermi line for the case shown in Figs. 1 and 2, namely, $B=0.45$, $\delta=0.25$, $\langle n\rangle=0.86$, and $T_c=94$ K.

solutions. We will return to this later.

It should be pointed out before leaving the discussion of our gap solutions that the coupling g in the BCS equation (1) is not a free parameter but was adjusted to get a $T_c\cong 100$ K, which is representative of the oxides $(g^2\chi_0=29)$. For the convenience of the reader the overlap of Fermi-surface contours and contours of zero gap for the case just described are shown in Fig. 5. It is clear that, while our solution has a small s-wave component in addition to the major $d_{x^2-y^2}$ component, the Fermi surface cuts the zero-gap contours at exactly four points as in the simpler and much studied pure $d_{x^2-y^2}$ case. Thus, we can expect the penetration depth to remain linear in temperature at low T and to change over to a T^2 dependence when resonant impurity scattering is introduced as in the pure $d_{x^2-y^2}$ case. Figure 5, however, does not show complete a- and b-axis symmetry and the absolute value of the penetration depth in these two directions will not be the same. To understand how the contours of zero gap, which are along the two main diagonals in pure $d_{x^2-y^2}$ symmetry, change their topology when a progressively larger extended s-wave component is introduced, it is helpful to look again at the contour shown in Fig. 5 and to realize that (using only the lowest harmonics) for an equal admixture of $d_{x^2-y^2}$ and extended s wave (s_x), the gap becomes dependent only on $\cos(K_x a)$ and therefore has its zeros along $K_x a=\pm\pi/2$, which are the two vertical lines on the figure. Note that there are four fixed points at $(K_x,K_y)=(\pm\pi/2,\pm\pi/2)$ where the gap vanishes whatever the choice of admixture because both the $d_{x^2-y^2}$ and the extended s part (s_x) are zero there. Also when we move to a pure extended s-wave (s_x) gap the zeros will have moved to lines crossing on the middle points of the Brillouin zone face and perpendicular to the main diagonals. This gives the full progression of the zero-gap contours as we go from pure $d_{x^2-y^2}$ to pure extended s wave (s_x). Only the lowest harmonics of Eq. (6) have been included for simplicity in the above discussion.

A quantity of considerable physical interest is the normal-state electronic density of states $N(\omega)$ as a function of energy ω. It is defined as

$$N(\omega)=\lim_{\Gamma\to 0}\frac{1}{\Omega}\frac{1}{\pi}\sum_K\frac{\Gamma}{(\epsilon_K-\omega)^2+\Gamma^2}\ . \tag{7}$$

In Fig. 6, we show a series of results for the case $\delta=0.25$, $\bar{t}=100$ meV, and a fixed value of $\bar{\mu}=2$, for various values of B, namely, $B=0.0$ (solid squares), 0.2 (solid circles), and 0.45 (solid triangles). For $B=0.0$ the band is symmetric about zero energy and we see that the familiar van Hove singularity at $\omega=0$ has split into two peaks symmetrically placed about $\omega=0$, which are much less pronounced than the single peak that exists in the more familiar (tetragonal) $\delta=0$ case. For $\bar{\mu}=2$ as we have chosen, the two split van Hove singularities are at $2\delta-8B$ and $-2\delta-8B$, respectively, in units of $\bar{t}$, and in these same units the top of the band is at $2(2+\delta)$. For positive values of B, the van Hove singularity shifts to lower energies, so that the band is no longer symmetric about $\omega=0$. Also it remains split into two singularities, the distance between them being 4δ, which is 100 meV for the case considered since $\delta=0.25$ and $\bar{t}=100$ meV.

The quasiparticle density of states in the superconducting state is also of interest. In principle it can be measured in quasiparticle tunneling experiments although these data often show considerable smearing of some unknown origin around the gap. This makes a critical com-

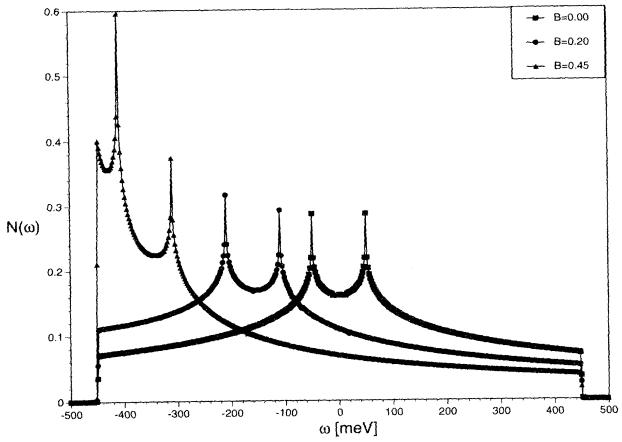

FIG. 6. The density of electron states $N(\omega)$ [Eq. (7)] as a function of energy ω in the normal state based on the dispersion relation (4) for $\delta=0.25$ and various values of B, the second-nearest-neighbor hopping. The solid squares are for $B=0.0$, solid circles for $B=0.2$, and solid triangles $B=0.45$. The chemical potential is $\bar{\mu}=2.0$ for all curves.

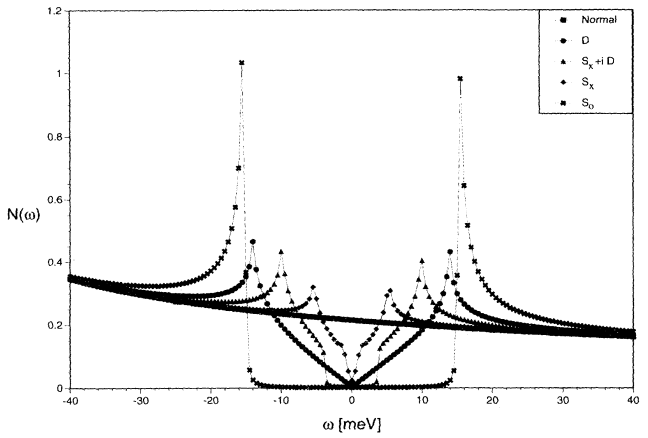

FIG. 7. The quasiparticle density of states $N_s(\omega)$ as a function of energy ω in the superconducting state [Eq. (8)] compared with the normal-state density of states (solid squares). The solid circles are for d wave, the solid crosses for conventional isotropic gap s_0, the solid diamonds for extended s-wave denoted by s_x, and the solid triangles for the case s_x+id. In all cases the gap is adjusted to get a T_c of 100 K assuming a ratio $2\Delta_0/k_BT_c$ of 3.5. The second-nearest-neighbor parameter $B=0.45$ and the filling is $\langle n\rangle=0.89$.

parison between theory and experiment for this quantity difficult. The quasiparticle density of states in the superconducting state, $N_s(\omega)$, is given by

$$N_s(\omega)=\lim_{\Gamma\to 0}\frac{1}{\pi}\frac{1}{\Omega}\sum_{K}\frac{\Gamma}{[E(\mathbf{K})-\omega]^2+\Gamma^2} \tag{8}$$

and results are shown in Fig. 7 for four cases. The normal-state results (solid squares) are also given for comparison. The solid circles are for a d wave of the form $[\cos(K_xa)-\cos(K_yb)]$, the diamonds are for an extended s wave (s_x) of the form $[\cos(K_xa)+\cos(K_yb)]$, the crosses for the usual s_0-wave, isotropic gap case, and finally the solid triangles are for a suggested form that comes from consideration of t-J models,[40–43] namely, s_x+id of the form

$$[\cos(K_xa)+\cos(K_yb)]+i[\cos(K_xa)-\cos(K_yb)]$$
$$\equiv\eta_{s_x}+i\eta_d\ . \tag{9}$$

We see that in the gap region around $\omega=0$ the extended s wave is much narrower than the d-wave case although they have exactly the same T_c value. Also, for s_x+id, a gap is predicted as $|\Delta_K|^2$ can vanish only if both real and imaginary parts simultaneously vanish on the Fermi surface. Such nodes occur only at four points halfway up the diagonal in the two-dimensional first Brillouin zero at $(\pm\pi/2a,\pm\pi/2a)$. A given Fermi surface will, in general, not cross these points. The graphs in this figure are for $B=0.45$ and $\delta=0$ with filling $\langle n\rangle=0.89$. The density of states curves are all at $T=0$ and the gap value was chosen in all cases to match a BCS value of $T_c=100$ K. In all these calculations and the corresponding one for the penetration depth, the gap value was taken to have BCS temperature variation of the form

$$\Delta_K(T)=\Delta_0\eta_i\tanh(1.75\sqrt{T_c/T-1})\ , \tag{10}$$

where $2\Delta_0/k_BT_c=3.52$. In Fig. 8 B and $\langle n\rangle$ remain the same as for Fig. 7 but now $\delta=0.25$ (asymmetric or orthorhombic case). Note that in the normal state the van Hove singularity (VHS) falls at $\omega\cong-12$ meV which is expected since $\bar{\mu}\cong0.51$ in this model and so the VHS should fall at $\bar{t}\,(2\delta-8B+4-2\bar{\mu})$. In the superconducting state the van Hove structure is shifted[44] to lower energies and falls below the main gap peak. We note that

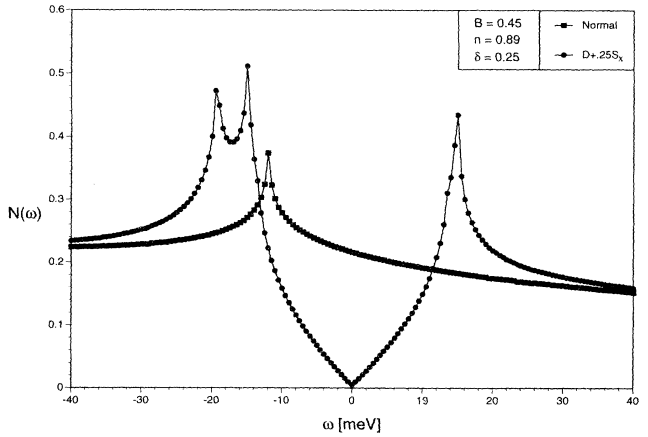

FIG. 8. The same parameters apply to Fig. 8 as do to Fig. 7 except $\bar{\mu}=0.51$ and the asymmetry parameter in the electron dispersion (4) is $\delta=0.25$ instead of zero. The solid squares are the normal state shown for comparison, while the solid circles are for the superconducting state $d+0.26s_x$, an admixture of d wave and extended s wave as given in Eq. (6), which is a very good approximation to the complete numerical solution of Fig. 2.

the density of state curve is not very different from a pure d wave although there is a 25% admixture of extended s wave. It would be difficult to detect this admixture in a tunneling experiment particularly as we often have smearing in the data of unknown origin. The reader may well wonder why we have not also shown the case when the full MMP numerical solutions are used to compute the density of states instead of using a combination of η_d and η_s. The full solution falls very close to the solid circles and was not shown on the figure as the difference would not show up clearly.

III. PENETRATION DEPTH

The penetration-depth tensor for specular reflection in the London limit $q \rightarrow 0$ is related to the electromagnetic field response function $K_{ij}(\mathbf{q},\omega)$ by

$$\lambda_{ij}(T)=\left[\frac{\mu_0}{4\pi}K_{ij}(0,0)\right]^{-1/2}, \tag{11}$$

where μ_0 is the permeability of free space. The current $J_i(\mathbf{q},\omega)$ is related to the electromagnetic vector potential $A^j(\mathbf{q},\omega)$ by

$$J_i(\mathbf{q},\omega)=-\sum_j K_{ij}(q,\omega)A^j(q,\omega)\ . \tag{12}$$

In the BCS mean-field approximation we can work out the expression for (11) and obtain the explicit form

$$\lambda_{ij}^{-2}(T)=\frac{4\pi e^2}{c^2}\frac{2}{\Omega}\sum_K V_{Ki}V_{Kj}\left[\frac{\partial f(E_{\mathbf{K}})}{\partial E_{\mathbf{K}}}-\frac{\partial f(\epsilon_{\mathbf{K}})}{\partial \epsilon_{\mathbf{K}}}\right], \tag{13}$$

where c is the velocity of light, Ω is the volume, and $v_{\mathbf{K}i}$ the electron velocity obtained from (3) as $\hbar v_{\mathbf{K}i}=\partial\epsilon_{\mathbf{K}}/\partial_{Ki}$.

At zero temperature, the first term in (13) does not contribute and for an infinite band, where $\epsilon_{\mathbf{K}}=\hbar^2K^2/2m^*$ with $\hbar$ Planck's constant and m^* the electron effective mass, we can work out (13) to be

$$\lambda_{ij}^{-2}(T=0)=\frac{4\pi e^2}{c^2}2\int N(\epsilon)d\epsilon\, v_{Ki}v_{Kj}\delta(\epsilon_k)$$
$$=\frac{4\pi e^2}{c^2}2N(0)\tfrac{1}{3}v_F^2\ , \tag{14}$$

where v_F is the Fermi velocity and $N(0)$ is the normal-state single-spin electron density of states at the Fermi surface. The electron density per unit volume is $n=\frac{2}{3}N(0)m^*v_F^2$ for free electrons and

$$\lambda^{-2}(T=0)=\frac{4\pi e^2}{c^2}\left[\frac{n}{m^*}\right], \tag{15}$$

which is the classical London penetration depth at zero temperature.

From a solution of the BCS gap equation (2) for a given band structure [Eq. (4)] and the MMP spin susceptibility of Eq. (1) we can easily evaluate (13) and present one of our many results in Fig. 9. In this figure, we show $\lambda_{xx}^{-2}(T)$ and $\lambda_{yy}^{-2}(T)$ for a MMP superconductor in arbitrary units as a function of temperature. The second-nearest-neighbor hopping parameter is $B=0.45$ and the filling $\langle n\rangle=0.88$ which corresponds to a chemical potential of $\bar{\mu}=0.51$. The coupling constant $g^2\chi_0$ in the BCS equation (2) was taken to have a value of 30.2 to get the right order of magnitude for T_c, namely, 94.0 K. The effective-mass anisotropy parameter in (4) was taken to be $\delta=0.25$, which leads to a 29% admixture of extended S wave plus constant part into the mainly d-wave gap on solution of the BCS equation. From the figure we conclude that the ratio $\lambda_{xx}^{-2}(T=0)/\lambda_{yy}^{-2}(T=0)$ is around 2 as in the experiments of Zhang *et al.*[18] We note also that both penetration depths λ_{xx}^{-2} and λ_{yy}^{-2} show a linear temperature variation at low T as is observed, although over the entire temperature range the agreement is not so good. In particular, the slope near T_c is smaller in our calculations than is observed. Simple BCS models of the kind used here seem not to be able to reproduce the detailed observations particularly near T_c. They omit, of course, any effect of fluctuations which could become important in this temperature region.

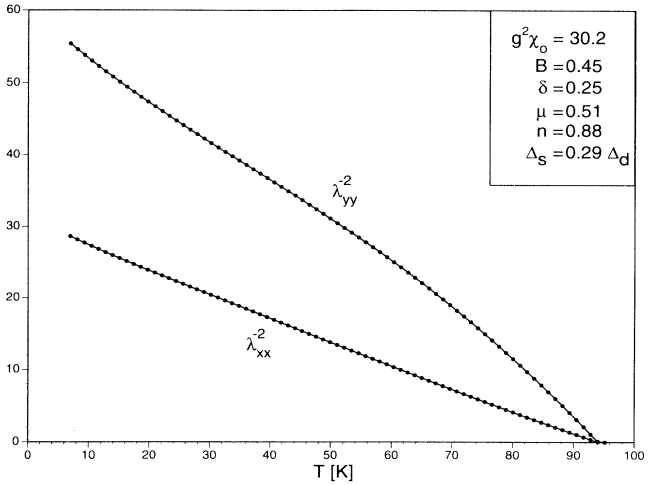

FIG. 9. Comparison of the temperature variation of the penetration depth (in arbitrary units) for x and y directions for the case $B=0.45$ (second-nearest-neighbor hopping), filling $\langle n\rangle=0.88$, $T_c=94$ K, and effective-mass anisotropy parameter and $\delta=0.25$. These results are based on complete numerical solutions of the BCS gap equation (2) for the MMP model susceptibility. The anisotropy in $\lambda_{ii}^{-2}(0)$ is about a factor of 2 between the a and b directions.

In Fig. 10, we show additional results in arbitrary units for a case with second-nearest-neighbor hopping $B=0.45$ a filling of $\langle n\rangle=0.89$ which corresponds to a chemical potential $\mu=0.51$ for three different effective-mass anisotropy parameters, namely, $\delta=0.05$, 0.15, and 0.25. In obtaining these curves, we did not use the full numerical solutions for the gap equation (2) based on the MMP susceptibility (1). Instead we approximated these by $\Delta_{\mathbf{K}}=\eta_d+\delta\eta_s$ of Eq. (6) which we found to be a reasonable approximate representation of the more complex complete numerical solutions. The complete solutions include many higher harmonics of $d_{x^2-y^2}$ and extended s-wave symmetry besides η_d and η_{s_x} of the simplified mod-

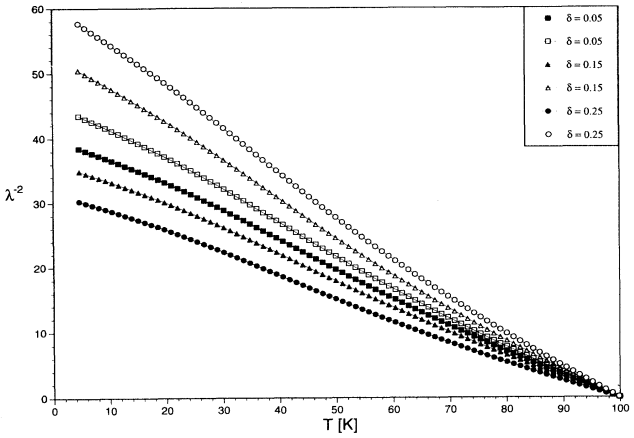

FIG. 10. Comparison of the temperature variation of the penetration depth (in arbitrary units) for y (open symbols) and x (solid symbols) directions for the case $B=0.45$ (second-nearest-neighbor hopping) and filling $\langle n\rangle=0.89$, for various values of δ, namely, $\delta=0.05$ (squares), 0.15 (triangles), and 0.25 (circles). In all cases $T_c=100$ K and the gap is set from $2\Delta_0/k_BT_c=3.5$ and a BCS temperature variation [Eq. (9)] is assumed. The gap is taken as a mixture of $d[\cos(K_xa)-\cos(K_yb)]$ and δ times extended $s[\cos(K_xa)+\cos(K_yb)]$.

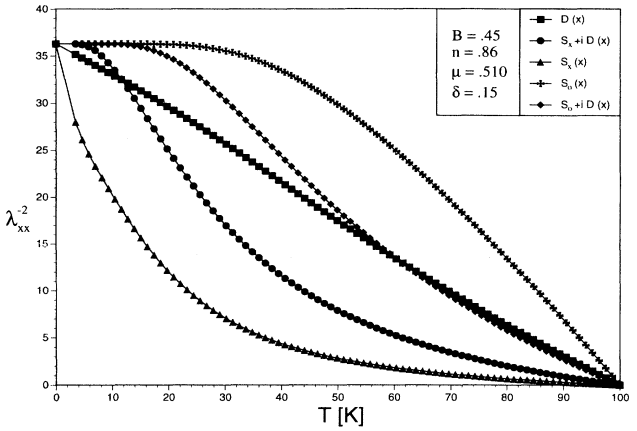

FIG. 11. The temperature dependence of the penetration depth (in arbitrary units) for various model gaps with an anisotropic band structure in the copper oxide plane. In all cases the second-nearest-neighbor hopping $B=0.45$, the filling $\langle n\rangle$ is 0.86, which corresponds to a chemical potential of $\bar{\mu}=0.51$, and $\delta=0.15$, which leads directly to anisotropy in the penetration depth. d stands for $[\cos(K_x)-\cos(K_y)]$, s for $[\cos(K_x)+\cos(K_y)]$, and s_0 for a constant. In all cases $T_c=100$ K and the gap is set from $2\Delta_0/k_BT_c=3.5$ with a BCS temperature variation. All the data are for λ_{xx} and similar data would apply for λ_{yy}. Squares are for d wave, the circles for s_x+id, the triangles for s_x, the diamonds for s_0+id, and the crosses for s_0.

el. The case with $\delta=0.25$ in Fig. 10 can be compared directly with the numerical results presented in Fig. 9 based on the full MMP solutions. While the results of the complete calculations for λ_{xx} (solid circles) show a slight concave downward curvature over a significant temperature range below T_c, the approximate solutions instead show a slight concave upward curvature (open circles) at the higher temperatures near T_c. These differences are small, however, and the approximate calculations certainly capture the qualitative behavior of the penetration depth very well. We can conclude that for some purposes the simple gap model of Eq. (6) is clearly sufficient and a full MMP calculation is not needed except in as much as it tells us that, for a given value of δ, we should mix in $d_{x^2-y^2}$ and δ times an extended s_x-wave part. While this rule applies reasonably well to all cases presented here, for other values of δ, filling, and chemical potential, the relationship between δ and the admixture of extended s_x and constant part can be much more complicated and a full numerical solution of the BCS gap equations is needed to get the correct admixture. Returning to the figure it is seen that the amount of anisotropy between the (xx) and the (yy) components of the zero-temperature penetration depth is a rapidly increasing function of the anisotropy parameter δ with a δ of only 0.25 giving almost a factor of 2 anisotropy. In Fig. 11, we show results of many more calculations of the penetration depth in arbitrary units for different models of the gap. In all cases the second-nearest-neighbor hopping parameter is $B=0.45$, the filling is $\langle n\rangle=0.86$, with chemical potential $\mu=0.51$, and the anisotropy parameter in the electron dispersion curve (4) is set at $\delta=0.15$ for all calculations. We present curves for λ_{xx} only. Those for λ_{yy} would be larger by about a factor of 2 (see Fig. 10). A constant isotropic gap (s_0) given by the crosses leads to a very flat low-temperature behavior below a reduced temperature of about $T/T_c\equiv t\cong 0.3$, reflecting an exponential activation region with a large finite gap everywhere on the Fermi surface. By comparison, the results for the s_0+id case (diamonds) show a definite finite gap but over a smaller temperature region as compared with the pure isotropic case, and the ones for s_x+id (solid circles) turn around and give a flat region only below $t\cong 0.1$. This is understandable because the case of constant gap plus i times $d_{x^2-y^2}$ does have a finite gap on the Fermi surface everywhere, because the real and imaginary parts of s_0+id can never vanish simultaneously, since s_0 never vanishes although it is smaller than for the corresponding pure isotropic gap case (s_0 alone) with the same T_c value equal to 100 K. This also applies to the s_x+id case, in which instance real and imaginary part can simultaneously vanish but only at four points on the two-dimensional CuO_2 plane Brillouin zone, namely, $(k_x,k_y)\equiv(\pm\pi/2a,\pm\pi/2a)$. But for a filling of $\langle n\rangle=0.86$ and $B=0.45$, $\delta=0.25$, the Fermi surface never crosses these four points although it does come close, and thus the effective minimum gap on the Fermi surface, while not zero, is nevertheless quite small, leading to an exponential activation region only at the lowest temperatures. The situation is quite different for the two remaining cases, namely, pure d wave (squares) and pure extended s wave s_x (triangles). In both these cases, there are gap zeros on the Fermi surface and the low-temperature behavior is radically modified to a linear law. The slope of this linear behavior, which is negative, is very much larger in absolute value for the extended s-

wave s_x case than it is for the $d_{x^2-y^2}$ case. This can be understood physically as follows. For the extended s-wave case s_x, the gap has zeros on lines bisecting the main diagonals of the two-dimensional CuO_2 Brillouin zone and cutting through the center of each of the four faces. This would also be the Fermi contour for $B=0$ and exactly half filling. In our case $B=0.45$ and the filling is slightly away from half filling with $\langle n \rangle = 0.86$ (see Fig. 5). In this case, the Fermi surface is slightly off the zeros of the extended s-wave gap function s_x but is still everywhere close and cuts it at a number of points. Because the gap on the Fermi surface is small everywhere compared with that of a d-wave superconductor with the same T_c value, the superfluid density increases much faster with increasing temperature and so the absolute slope of the inverse square of the penetration depth, which is proportional to the superfluid density, is very large. The curvature of the resulting curve when viewed over the entire temperature range shown is concave up. This also applies for the same reasons to the s_x+id (solid circles) case but in that case there is a turnover at low temperature to the exponentially activated regime.

Our single-band model was designed to account, as a first step, for the orthorhombic nature of YBCO. The orthorhombic symmetry in this system has its origin in the existence of CuO chains which lie in a different plane from the CuO_2 plane. Our model presumably applies best if the chain and plane bands are significantly hybridized and, in a sense, represents the opposite limit of an independent chain and plane model. For two independent bands, we would expect a very distinct temperature dependence for the in-plane penetration depth in a and b directions because the screening currents in one direction would involve the chains while they would not be involved in the other direction. This is to be contrasted with our model, which predicts a similar temperature variation in both directions, as is observed experimentally. The absolute values of λ_a and λ_b are, of course, quite different.

Different sources of anisotropy can have quite different consequences. For $Bi_2Sr_2CaCu_2O_{8+\delta}$ (Bi 2:2:1:2), there exists a superlattice modulation which lifts the tetragonal symmetry. Inasmuch as this superlattice modulation may not have a strong effect on the resulting Fermi surface, we would not expect λ_a and λ_b to be very different in this case, although a detailed calculation would be required to answer the question definitively.

IV. SUMMARY AND CONCLUSIONS

The penetration depth in $YBa_2Cu_3O_{7-\delta}$ is found to be linear in temperature at low temperature, which is characteristic of a gap with nodes on the Fermi surface. The zero-temperature in-plane penetration depth is highly anisotropic with $\lambda_a(T=0)=1600$ Å and $\lambda_b(T=0)=1030$ Å. This anisotropy cannot be understood in simple models of a single CuO_2 plane with tetragonal symmetry; and has been taken as evidence that a significant fraction of the condensate resides in the CuO chains. To include the chains as well as CuO_2 planes would require, at minimum, the use of a two-band model, one for the planes and the other for the chains. Instead of dealing with such a complication, we have opted here to retain the simplicity of a single band but have attempted to introduce the anisotropy of the realistic band structure through an anisotropic first-nearest-neighbor hopping which is taken to be different in a and b directions. While this simple model is not expected to be quantitatively correct, it does allow in a simple way for the possibility of $\lambda_a(0)\neq\lambda_b(0)$. In fact, we found that an anisotropy in nearest-neighbor hopping of about 25% is quite sufficient to explain the factor of 1.6 observed for the ratio of λ_a to λ_b at $T=0$.

A very important feature of the anisotropy introduced in the tight-binding band for the CuO_2 plane is that the gap is found to be an admixture of three irreducible representations of the tetragonal point group, namely, $d_{x^2-y^2}$ extended s wave, and a constant part. For the orthorhombic group these three functions belong, of course, to the same irreducible representation. So the result that they mix when chains are included is not surprising, since we then effectively have orthorhombic symmetry. The correct admixture of the three representations, however, cannot be determined from general group-theoretical arguments alone. Here we determine this admixture through the BCS gap equation, written for a nearly antiferromagnetic Fermi liquid with pairing due to exchange of antiferromagnetic spin fluctuations in the CuO_2 plane. For the pairing interaction in these equations we use the phenomenological spin susceptibility of Millis, Monien, and Pines which gives a good description of the spin dynamics in the tetragonal CuO_2 plane. It is used here without changes and therefore introduces no parameters, since MMP have fitted it to the NMR data and we make no modification in this quantity. The band structure used in Eq. (2), however, does not have tetragonal symmetry so the resulting gap solutions are no longer pure $d_{x^2-y^2}$ as stated before. The admixture of extended s wave changes the zero-gap contours which no longer fall along the two main diagonals as is the case for pure $d_{x^2-y^2}$ symmetry. Nevertheless, the gap still goes to zero at four points on the Fermi surface and we have found that the anisotropic penetration depth $\lambda_a(T)$ and $\lambda_b(T)$ separately exhibit a linear temperature dependence at low T as found experimentally although, over the entire range of temperature, the agreement of our BCS calculations with the experimental results is not quantitative. Nevertheless, some of the main features of the data can easily be explained even though our model has been very simple. Further progress will probably require the development of more complicated multiple-band models which we hope to study in the future. Also it will be necessary to study the effect of normal elastic impurity scattering for the mixed-symmetry case. In this case the impurities enter both the gap and the normal-state renormalization channels in contrast to the pure d-wave case, where they do not make a contribution to the gap channel.

ACKNOWLEDGMENTS

This work was supported by the Natural Sciences and Engineering Research Council of Canada (NSERC) and by the Canadian Institute for Advanced Research (CIAR).

[1]W. N. Hardy, D. A. Bonn, D. C. Morgan, R. Liang, and K. Zhang, Phys. Rev. Lett. **70**, 3999 (1993).
[2]D. A. Bonn *et al.*, Phys. Rev. B **47**, 11 314 (1993).
[3]D. A. Bonn, P. Dosanjh, R. Liang, and W. N. Hardy, Phys. Rev. Lett. **68**, 2390 (1992).
[4]K. Zhang, D. A. Bonn, R. Liang, D. J. Barr, and W. N. Hardy, Appl. Phys. Lett. **62**, 3019 (1993).
[5]D. A. Bonn, K. Zhang, R. Liang, D. J. Barr, and W. N. Hardy, J. Supercond. **6**, 219 (1993).
[6]W. N. Hardy, S. Kamal, D. A. Bonn, K. Zhang, R. Liang, E. Klein, D. C. Morgan, and D. J. Barn, Physica B **197**, 609 (1994).
[7]B. G. Levi, Phys. Today **46** (5), 17 (1993).
[8]H. Ding, J. C. Campuzano, K. Gofron, C. Gu, R. Liu, B. W. Veal, and G. Jennings, Phys. Rev. B **50**, 1333 (1994).
[9]C. G. Olson *et al.*, Science **245**, 731 (1989).
[10]Z. X. Shen *et al.*, Phys. Rev. Lett. **70**, 1553 (1993).
[11]D. S. Dessau, Z. X. Shen, B. O. Wells, and W. E. Spicer, J. Phys. Chem. Solids **52**, 1401 (1991).
[12]D. A. Wollman, D. J. Van Harlingen, W. C. Lee, D. M. Ginsberg, and A. J. Leggett, Phys. Rev. Lett. **71**, 2134 (1993).
[13]P. Chaudhari and Shawn Yu Lin, Phys. Rev. Lett. **72**, 1084 (1994).
[14]A. G. Sun, D. A. Gajewki, M. B. Maple, and R. C. Dynes, Phys. Rev. Lett. **72**, 2267 (1994).
[15]S. Chakravarty, A. Sudbo, P. W. Anderson, and S. Strong, Science **261**, 337 (1993).
[16]P. B. Littlewood and C. M. Varma, Phys. Rev. B **46**, 405 (1992).
[17]A. A. Abrikosov, Physica C **182**, 191 (1991).
[18]K. Zhang, D. A. Bonn, S. Kamal, R. Liang, D. J. Baar, W. N. Hardy, D. Basov, and T. Timusk, Phys. Rev. Lett. **73**, 2484 (1994).
[19]D. N. Basov, R. Liang, D. A. Bonn, W. N. Hardy, B. Dabrowski, M. Quijada, D. B. Tanner, J. P. Rice, D. M. Ginsberg, and T. Timusk, Phys. Rev. Lett. **74**, 598 (1995).
[20]N. E. Phillips, J. P. Emerson, R. A. Fisher, J. E. Gordon, B. F. Woodfield, and D. A. Wright, J. Supercond. **7**, 251 (1994).
[21]V. Z. Kresin and S. A. Wolf, Phys. Rev. B **46**, 6458 (1992).
[22]V. Z. Kresin and S. A. Wolf, Physica C **198**, 328 (1992).
[23]T. A. Friedmann *et al.*, Phys. Rev. B **42**, 6217 (1990).
[24]J. L. Cohn *et al.*, Phys. Rev. B **45**, 13 144 (1992).
[25]R. Gagnon, C. Lupien, and L. Taillifer, Phys. Rev. B **50**, 3458 (1994).
[26]R. C. Yu, M. B. Salamon, J. P. Lu, and W. C. Lee, Phys. Rev. Lett. **69**, 1431 (1992).
[27]H. Krakauer, W. E. Pickett, and R. E. Cohen, J. Supercond. **1**, 111 (1988).
[28]W. E. Pickett, R. E. Cohen, and H. Krakauer, Phys. Rev. B **42**, 8764 (1990).
[29]W. E. Pickett, H. Krakauer, R. E. Cohen, and D. J. Singh, Science **255**, 1 (1992).
[30]H. Haghighi *et al.*, Phys. Rev. Lett. **67**, 382 (1991).
[31]A. J. Arko *et al.*, Phys. Rev. B **40**, 2268 (1989).
[32]V. C. Campuzano *et al.*, Phys. Rev. Lett. **64**, 2308 (1990).
[33]N. Schroeder *et al.*, Phys. Rev. B **47**, 5287 (1993).
[34]G. Kido *et al.*, in *Advances in Superconductivity III,* edited by H. Kajimura and H. Hayakawa (Springer-Verlag, Tokyo, 1991), p. 237.
[35]D. B. Tanner and T. Timusk, in *Physical Properties of High Temperature Superconductors III,* edited by D. M. Ginsberg (World Scientific, Singapore, 1992), p. 363.
[36]P. B. Allen, W. E. Pickett, and H. Krakauer, Phys. Rev. B **37**, 7482 (1988).
[37]A. J. Millis, H. Monien, and D. Pines, Phys. Rev. B **42**, 167 (1990).
[38]St. Lenck, J. P. Carbotte, and R. C. Dynes, Phys. Rev. B **49**, 6933 (1994).
[39]St. Lenck and J. P. Carbotte, Phys. Rev. B **49**, 4176 (1994).
[40]Q. P. Li and Robert Joynt, Phys. Rev. B **47**, 531 (1993).
[41]G. Kotliar, Phys. Rev. B **37**, 3664 (1988).
[42]G. J. Chen, Robert Joynt, F. C. Zhang, and C. Gros, Phys. Rev. B **42**, 2662 (1990).
[43]M. V. Ubbens and P. A. Lee, Phys. Rev. B **46**, 8434 (1992).
[44]C. Zhou and H. J. Schulz, Phys. Rev. B **45**, 7397 (1992).